Transcriptome Dynamics in Mouse Amygdala under Acute and Chronic Stress Revealed by Thiol-labeled RNA Sequencing

Dan Zhao[1#], Lu Zhang[1#], Yang Yang[1,2*]

1. School of Life Science and Technology, ShanghaiTech University, Shanghai 201210, China.

2. State Key Laboratory of Advanced Medical Materials and Devices, ShanghaiTech University, Shanghai 201210, China

# These authors contributed equally to this work

* Correspondence: yangyang2@shanghaitech.edu.cn

Abstract

Both acute and chronic stress have significant impact on brain functions. The amygdala is essential in mediating stress responses, but how its transcriptomic dynamics change under stress remains elusive. To overcome the difficulties in detecting subtle stress-induced changes by evaluating total RNA using classic RNA sequencing, we conducted thiol-labeled RNA sequencing (SLAM-seq). We injected 4-thiouridine (4sU) into mouse amygdala followed by SLAM-seq to detect nascent mRNA induced by acute and chronic restraint stress, and found that SLAM-seq could label actively transcribed genes in the major neuronal and glial subtypes. We also found that acute stress induced active transcription of 6 gamma-aminobutyric acid (GABA) receptors and only 1 glutamate receptor, indicating an imminent increase of inhibitory control in the stressed amygdala. Conversely, chronic stress led to active transcription of 3 glutamate receptors and 4 GABA receptors, suggesting a release of inhibitory control and hyperactivity of the amygdala. SLAM-seq also identified genes associated with myelination under chronic stress, and this finding is confirmed by immunostaining showing increased myelination in chronically stressed amygdala. Additionally, genes detected by SLAM-seq and RNA-seq only partially overlapped, with SLAM-seq particularly sensitive to transcriptional changes in genes with high basal transcription levels. Thus, by applying SLAM-seq *in vivo*, we obtained a rich dataset of nascently transcribed genes in the amygdala under stress, and revealed distinct transcriptional dynamics associated with acute and chronic stress.

Introduction

The impact of stress on the brain is profound and has been linked to an increased risk of mental illnesses, including depression and anxiety disorders [1, 2]. Both acute and chronic stress can induce adaptive changes in various brain regions [3-9], including the amygdala, which plays a key role in processing physiological and behavioral responses to stress [10, 11]. In its resting state, the amygdala is tightly regulated through inhibitory mechanisms mediated by gamma-aminobutyric acid (GABA) [12]. Previous research showed that stress leads to amygdala disinhibition, resulting in its heightened activity [13, 14]. While many studies have demonstrated that stress affects amygdala function, the underlying molecular mechanisms responsible for these changes remain elusive. To understand the stress-induced effects in the amygdala at the molecular level, it is essential to study how gene expression in amygdala is influenced by acute and chronic stress.

It has long been established that neuronal activities lead to fast expression of immediate early genes, which further regulates transcription of thousands of downstream genes over an extended period [15-17]. Such activity-dependent transcription dynamics are crucial for modulating neuronal functions and long-term connectivity changes [18, 19]. Studies have shown that glial cells in the brain also exhibit significant functional changes induced by neuronal activities. For example, oligodendrocytes undergo activity-dependent myelination [20, 21]. However, the abundance of gene transcripts for maintaining cellular functions, and the complex morphology of neurons and glia, made the classic RNA sequencing (RNA-seq) method unsuitable for studying the dynamic transcriptomic changes of these cells [22].

The thiol-labeled RNA sequencing (SLAM-seq) method specifically label newly transcribed mRNAs [23], and has been widely applied in cultured cells [24, 25]. Recently, SLAM-seq has also been extended to *in vivo* studies to explore genomic changes during zebrafish embryo development [26], and to identify cell type-specific transcriptome in mouse tissues in a Cre-dependent manner (SLAM-ITseq, [27]). Although SLAM-ITseq provides a solution to metabolically label RNA with 4-thiouracil (4-TU) in a specific cell type *in vivo*, this method requires usage of double-transgenic mouse lines to achieve cell type-specific expression of uracil phosphoribosyltransferase (UPRT), to transform 4-TU to 4-thiouridine (4sU) in Cre-expressing cells, limiting the applicability.

By conducting SLAM-seq with direct stereotactic injection of 4sU, we detected newly transcribed genes in the amygdala under acute and chronic stress. Bioinformatic analyses showed that the injected 4sU was integrated into the transcription of genes expressed in major brain cell types. In addition, acute stress and chronic stress induced differential transcription of GABA and glutamate receptors, indicating diverse inhibitory control in the amygdala under acute and chronic stress. Furthermore, compared to RNA-seq, SLAM-seq is more sensitive to transcriptional changes in genes expressed in high basal levels.

Results

Adapt SLAM-seq for the brain through stereotactic injection of 4sU

Neuronal activity is known to quickly trigger the transcription of many genes [15-17]. Seeking to detect gene transcription in response to diverse conditions of neuronal activity in different brain regions, we adapted the SLAM-seq protocol *in vivo* by injecting 4sU directly into the brain region of interest. The stereotactic injection method was used to ensure the target delivery of 4sU, a nucleotide analog that can be imported into animal cells by equilibrate nucleoside transporters [28], in selected brain regions (See Methods for details). To estimate the 4sU incorporation rate in brain cells, we first injected 4sU (100mM, dissolved in 10% DMSO, 1uL) into the mouse auditory cortex (**Fig. 1a**), and performed biotin dot blot essay with mRNAs extracted from the cortex at 2 h, 8 h, and 24 h after 4sU injection [29]. The labeling strength increased with labeling time (**Fig. 1b**), and at 24 h post injection, the labeling is highly efficient. Thus, we determined that 24 h is a sufficient duration to allow 4sU diffusion into brain cells to support SLAM-seq.

To evaluate the extent of tissue damage potentially caused by the injection of 4sU, we used TUNEL (Terminal deoxynucleotidyl transferase dUTP Nick End Labeling) staining to assess cell death in the injected brain region [30]. We injected 4sU (100mM, dissolved in 10% DMSO, 1uL) and DMSO (10%, 1uL) into the mouse auditory cortex and amygdala, and 24 h later, extracted the mouse brains for slicing and TUNEL staining (Methods). We did not see dead cells in the brain slices near the injection sites, for both 4sU and DMSO injections, suggesting that neither 4sU nor DMSO induced detectable cell death or tissue damage in the injected brain regions (**Fig. 1c, Supp. Fig. 1**).

92 We also assessed whether the presence of 4sU had any impact on the transcriptome by performing
93 150bp paired-end sequencing of total mRNA extracted from the isolated mouse auditory cortex
94 and amygdala at 24 h after stereotactic 4sU or DMSO injections (**Supp. Fig. 2a, 2b**). By comparing
95 the read counts for all genes [23], we did not observe any significant difference in gene expression
96 levels between 4sU (denoted as 4sU+) and DMSO (denoted as 4sU-) groups (**Fig.1d, Supp. Fig.**
97 **2c**). These findings support that local injection of 4sU into specific brain regions enables efficient
98 incorporation into transcription in brain cells, without obviously affecting the gene expression.
99
100 **Identify 4sU-incorporated mRNA with SLAM-seq under basal conditions**
101 Recently, in addition to cultured cells [24, 25], SLAM-seq has also been applied *in vivo* by
102 injecting 4sU into zebrafish embryo [26], or injecting 4-thiouracil (4-TU) intraperitoneally into
103 transgenic mice expressing UPRT in selected cell types [27]. Given that local injection of 4sU into
104 the mouse brain has never been reported, we needed to empirically determine whether the
105 delivered 4sU can be incorporated into the nascently transcribed RNA molecules. We injected 4sU
106 (100mM, 1uL, dissolved in 10% DMSO) and DMSO (10%, 1uL) into the mouse amygdala 24 h
107 prior to tissue dissection and RNA extraction (**Fig. 2a**), to establish a baseline (BL) for nascent
108 RNA transcription in normal behaving mice. We then subjected the aforementioned total RNA
109 extracts to iodoacetamide (IAA) treatment (Methods, **Supp. Fig. 3a**), to covalently attach a
110 carboxyamidomethyl group to 4sU by nucleophilic substitution [23], and then performed 150bp
111 paired-end RNA-seq (**Supp. Fig. 3b**). During the reverse transcription step of RNA-seq library
112 preparation, a guanine (G), instead of an adenine (A), is base paired to an alkylated 4sU, leading
113 to the thymine (T) to cytosine (C) base conversion (T>C conversion) at the corresponding T
114 position in mRNA [23]. To control for the background T>C conversion rate without 4sU, RNA
115 obtained from DMSO-injected amygdala was subjected to the same procedures before RNA-seq.
116
117 We calculated the T>C conversion rates for each gene in both the 4sU-injected and DMSO-injected
118 samples using SLAM-DUNK software [31]. At the whole transcriptome level, the average T>C
119 conversion rate of the 4sU-injected group was significantly higher than that of DMSO-injected
120 group (**Fig. 2b**), indicating that the injected 4sU was incorporated into transcription. We identified
121 414 genes with significantly higher T>C conversion rates in the 4sU group than in the DMSO
122 group (**Fig. 2c**), which can be plausibly interpreted as genes undergoing active transcription. Note

that these mice were not subjected to any behavioral or physiological perturbations, therefore, the 414 differentially 4sU-labeled genes were actively transcribed under normal baseline conditions. Indeed, these genes included sodium channels (*Scn1b*), potassium channels (*Kcnab2, Kcnc2*), cation transport ATPases (*Atp1a2, Atp1b2)*, calcium channels (*Cacng7*) and Calmodulin (*Calm3*), all of which are essential for maintaining basic neuronal functions [32].

Determine the 4sU labeling efficiency in distinct cell types

Identification of genes encoding neuron-specific ion channels indicated that 4sU was successfully incorporated into transcription of genes in the amygdala neurons. To additionally evaluate the efficiency of 4sU incorporation into the transcription of other cell types in amygdala, we cross-referenced the 414 differentially 4sU-labeled genes with known marker genes of major cell types as reported in single-cell RNA sequencing studies [33, 34]. We found that the 414 differentially labeled genes under baseline conditions covered marker genes of excitatory (*Slc17a7, Camk2a*) and inhibitory neurons (*Gad1, Gad2*), astrocytes (*Gfap, S100b*), microglia (*Fcer1g, Lyz2*) and oligodendrocytes (*Mobp, Plp1*). The T>C conversion rates of these genes were significantly higher in 4sU-injected than DMSO-injected amygdala (**Fig. 2d**). These results indicate that 4sU has been imported into major neuronal and glial cell types of the amygdala, and could be effectively incorporated into the transcription of these cells to signal nascent transcription.

Transcriptome dynamics of the amygdala under acute stress

The amygdala has been extensively implicated in stress responses [10, 11]. To identify genes that were actively transcribed upon acute stress (AS), we subjected 4sU- and DMSO-injected mice to 1.5 h of restraint stress [35], and immediately after the stress treatment, we isolated the amygdala and extracted total RNAs (Methods, **Fig. 3a**). We treated the RNA samples with IAA for SLAM-seq, and identified the differentially 4sU-labeled genes using SLAM-DUNK by comparing T>C conversion rates between 4sU- and DMSO-injected amygdala samples (**Supp. Fig. 4a**). Meanwhile, we conducted a separate bulk RNA-seq analysis, using DESeq2 software package [36] to identify differentially expressed genes (DEGs) in acute stress condition, compared to baseline.

By comparing the T>C conversion rates of genes between the 4sU and DMSO groups under AS, we identified 728 differentially 4sU-labeled genes with significantly higher T>C conversion rates

154 in the 4sU group (FDR<0.05, $\log_2$FC>1, **Fig. 3b**. FDR: false discovery rate. FC: fold change). A
155 gene ontology (GO) analysis of the differentially 4sU-labeled genes in the AS samples indicated
156 enrichment for terms including "vesicle-mediated transport in synapse", "regulation of
157 neurotransmitter levels", and "synaptic vesicle cycle", all of which are closely associated with
158 synaptic vesicle functions (**Fig. 3c, Supp. Fig. 4b**). Among these are genes tightly linked to
159 synaptic vesicle release, including *Git1, Syn1, Synj1* [37-39] (**Fig. 3b**). GO analysis also revealed
160 enrichment for terms such as "regulation of synaptic plasticity" and "learning or memory", and
161 related genes included *Vgf, Prkcg, Snap25, Snap47* [40-42] (**Fig. 3b, 3c**).
162
163 A KEGG pathway analysis showed that the most significant pathways include "glutamatergic
164 synapse" and "GABAergic synapse", suggesting that AS had a strong influence on both excitatory
165 and inhibitory synaptic functions (**Fig. 3d**). Comparing genes identified under BL condition with
166 genes identified under AS, we found only one GABA receptor gene (*Gabra1*) among the
167 differentially 4sU-labeled genes under BL, in contrast to 6 GABA receptor genes under AS
168 (*Gabbr1, Gabra1, Gabra3, Gabrb2, Gabrg1, Gabrg2*), representing a higher transcription rate for
169 GABAergic receptors in the amygdala after acute stress. Conversely, only one glutamate receptor
170 gene (*Grina*) was detected under AS, and none under BL (**Fig. 3e**). Consistent with previous
171 studies linking amygdala GABAergic inhibitory control to stress response [14, 43], our results
172 suggested a strong influence on GABAergic neurons in the amygdala by acute stress, in the form
173 of quickly elevating GABA receptor expression.
174
175 **Sensitivity of SLAM-seq vs. RNA-seq**
176 Neurons require high abundance of transcripts for maintaining normal functions, while also exhibit
177 highly dynamic activity-induced transcription, making it hard to detect the subtle changes by
178 evaluating the total RNA amount using classic RNA-seq [22]. Indeed, none of the differentially
179 4sU-labeled GABA receptor and glutamate receptor genes identified by SLAM-seq were detected
180 using the differential gene expression analysis, even with a lenient standard (FDR<0.1,
181 Log_2FC>0.1, **Fig. 3f, Supp. Fig. 4c**). In total, 374 significantly upregulated and 279 downregulated
182 genes were identified using DESeq2 by comparing RNA read counts between AS and BL
183 conditions. 44 overlapping genes were identified by intersecting these AS-upregulated genes with
184 differentially 4sU-labeled genes under AS (**Fig. 3g**). These genes include known stress-related

genes such as *Cldn11, Vamp1, Glud1* and *Etnppl* [44-47]. For all of the overlapped genes, fold change is bigger for SLAM-seq analysis than RNA-seq (**Fig. 3h**).

Further investigation revealed that the overlapped genes detected by SLAM-seq and RNA-seq had relatively high expression levels (**Fig. 3i, Supp. Fig. 4d**). In fact, the genes with very high expression levels that were marginally upregulated as determined by DESeq2 (Log_2FC <0.5) were detected by SLAM-seq (red data points in **Fig. 3i**) with bigger fold changes and higher significance levels (**Fig. 3h, k**). In addition, genes identified by SLAM-seq had higher expression levels than genes detected by RNA-seq (**Fig. 3j**, Kolmogorov-Smirnov test, $p < 0.05$). These results suggest that compared to RNA-seq, SLAM-seq is more sensitive to genes with high expression levels, and is therefore useful for detecting the increased active transcription of genes that can be masked by the high abundance of transcripts required for normal functioning. This is of particular importance for neurons, given the high basal expression level of many genes [22].

Transcriptome dynamics of amygdala under chronic stress

Chronic stress (CS) poses prolonged impact in the brain [48]. For chronic stress experiments, we subjected mice to 7 days of restraint stress, 2 h each day [49, 50] (Methods, **Fig. 4a**). To examine the long-lasting transcriptomic changes under CS, we extracted the amygdala at 10 h after the final restraint stress session on day 7. We reasoned that by shifting 10 h, we reduced the possibility of detecting acute changes induced by the last session of restraint stress. 4sU was injected into the amygdala 24 h before brain extraction, same as BL and AS experiments. By comparing T>C conversion rates between 4sU and DMSO injected groups, we identified 815 differentially 4sU-labeled genes under CS (**Fig. 4b, Supp. Fig. 5a**). We performed a GO analysis for these genes, and found that in addition to terms associated with neuronal functions such as “synaptic vesicle cycle” and “neurotransmitter secretion”, there is also enrichment for terms closely linked to glial cells, especially oligodendrocytes and microglia (**Fig. 4c**). These terms include “myelination”, “ensheathment of neurons” and “axon ensheathment”, which are tightly linked to the function of oligodendrocytes, as well as “autophagy” and “autophagosome”, which are associated with microglia (**Supp. Fig. 5b**). Among these genes, *Mag* and *Dag1* are associated with myelination, and *Rragb* and *Usp36* are associated with autophagy [51].

216 Regarding sensitivity for SLAM-seq vs. RNA-seq, we noted a similar trend for CS data to AS.
217 DESeq2 analysis detected 53 significantly up-regulated and 11 down-regulated genes for CS
218 (FDR<0.1, Log_2FC>0.1, **Fig. 4d**). Intersection of the differentially 4sU-labeled genes identified
219 by SLAM-seq and upregulated genes identified by RNA-seq revealed 11 overlapping genes (**Fig.**
220 **4e**), all with high expression levels (**Fig. 4f, Supp. Fig. 5c**). Expression of six out of the 11
221 overlapped genes is affected by chronic stress (*Esrrg, Gabarapl2, Cct8, Vamp1, Nrsn1, Cplx1*) [47,
222 52-54]. These genes all show bigger fold changes and 9 out of 11 genes also show higher
223 significance levels for SLAM-seq than for RNA-seq (**Fig. 4h, 4i**). Similar to AS, genes identified
224 by SLAM-seq in CS also had higher expression levels (**Fig. 4g**, Kolmogorov-Smirnov test, $p <$
225 0.05), again demonstrating the sensitivity of SLAM-seq for detecting actively transcribed genes
226 with high abundance. The GO analysis of the genes identified by SLAM-seq indicated enrichment
227 for terms closely linked to glial functions, but these terms did not show in GO analysis of genes
228 identified by RNA-seq (**Supp. Fig. 6**). Thus, the low-magnitude yet persistent transcriptome
229 changes associated with CS are more likely to be captured by SLAM-seq.
230
231 **Comparison of differentially 4sU-labeled genes among BL, AS and CS conditions**
232 By comparing the differentially 4sU-labeled genes under BL, AS and CS conditions, we found that
233 a majority of genes (363 out of 413) labeled under BL were also identified in either AS or CS
234 conditions, including known housekeeping genes such as *Sdha, Ywhaz*, *Gfap* [55] (**Fig. 5a**). These
235 genes were actively transcribed regardless of stress conditions, indicating their important roles in
236 maintaining normal cellular functions. In contrast to BL, we identified many more condition-
237 specific genes after stress treatments, namely, 224 AS-specific genes and 333 CS-specific genes
238 (**Fig. 5a**). Among the 172 AS-CS overlapped genes, 29 were associated with synaptic transmission,
239 synaptic vesicle cycle and synaptic regulations (**Fig. 5a**). Thus, both acute and chronic stress
240 strongly affected synaptic functions in amygdala neurons. Notably, compared to CS, AS triggered
241 active transcription of a higher proportion of synapse-related genes, among which were genes
242 associated with protein localization to postsynaptic membrane (*Git1, Mapk10, Stx1b, Kif1a*) [39,
243 56, 57], highlighting immediate postsynaptic plasticity caused by acute stress (**Fig. 5b**).
244
245 As described in an earlier section, we detected 6 GABA receptor genes (*Gabbr1, Gabra1, Gabra3,*
246 *Gabrb2, Gabrg1, Gabrg2*) and 1 glutamate receptor gene (*Grina*) under AS, representing an

247 imminent effect of AS on GABAergic inhibitory control of the amygdala. In comparison, we found
248 4 GABA receptor genes (*Gabbr1, Gabra1, Gabra3, Gabrg2*) and 3 glutamate receptor genes
249 (*Gria3, Gria4, Grina*) among the differentially 4sU-labeled genes under CS (**Fig. 5c**). The increase
250 in excitatory receptor transcription and relatively lower transcription of GABAergic receptors
251 might underlie hyperactivity of the amygdala [13, 14], caused by stress-induced removal of
252 GABAergic inhibitory control.
253

254 **Validation of SLAM-seq results by quantitative immunofluoresence**

255 Recent studies suggested that elevated neuronal and axonal activity could trigger myelination [20,
256 21], a phenomenon known as "activity-dependent myelination". In line with these results, CS-
257 specific genes detected by SLAM-seq included a large proportion of genes related to myelination,
258 including *Fyn, Dag1, Mag, Epb41l3,* and *Ndrg1* (**Fig. 5d**), and the enriched GO terms included
259 "myelination", "positive regulation of myelination", and "myelin sheath" (**Fig. 5e**). These genes
260 were not detected by RNA-seq (**Supp. Fig. 7**), possibly due to their high baseline expression levels.
261 To examine whether the increased transcription of myelination related genes after CS is indicative
262 of increased myelination in the amygdala, we stained brain slices of chronically stressed mice and
263 control mice with a myelin marker, the myelin basic protein (MBP), and compared the
264 immunofluorescence signal intensity between the two groups (**Fig. 5f**). We found that MBP signal
265 is indeed significantly stronger in the chronically stressed amygdala than the control ($p<0.01$,
266 Student's t-test, **Fig. 5g**), validating the SLAM-seq results that chronic stress led to increased
267 myelination in the mouse amygdala.
268

269 **Discussion**

270 By directly injecting 4- thiouridine (4sU) into the amygdala followed by SLAM-seq, we were able
271 to identify newly transcribed genes under acute and chronic stress. By cross-referencing these
272 genes with known cell type-specific marker genes, we found that the injected 4sU was integrated
273 into the transcription of major subtypes of neurons and glia cells in the amygdala. Analyses
274 revealed that acute stress resulted in increased transcription of GABA receptors in neurons, while
275 chronic stress had a stronger impact on transcription of glutamate receptors and genes associated
276 with myelination, both in line with heightened activity of the amygdala [14]. Furthermore, we
277 observed that SLAM-seq exhibited greater sensitivity to transcriptional changes in genes with high

278 expression levels compared to RNA-seq. Thus, by applying SLAM-seq to the amygdala, we
279 generated a rich dataset which can be used in future studies to dissect the functions of genes related
280 to stress responses.
281
282 Neurons have highly specialized morphology, including axons and dendrites that can span long
283 distances, with functional subcellular compartments such as dendritic spines and axonal boutons
284 [58]. The transcriptional networks in neurons are dynamically modulated by synaptic activities,
285 through coupling of a small subset of active synapses to the nucleus [59, 60]. Given the abundance
286 of gene transcripts for maintaining fundamental neuronal functions such as action potential firing
287 [19], the transcriptional modulation that lead to activation of relevant gene expression may not
288 alter the total mRNA of these genes [22]. Therefore, the most common method for gene expression
289 profiling, RNA-seq, may not be suited for accessing the highly dynamic transcriptional changes
290 under fast-varying physiological, behavioral or pathological conditions.
291
292 SLAM-seq, a metabolic RNA labeling method for identifying newly synthesized RNA molecules,
293 is an alternative approach to gain insights into the transcriptional regulation regardless of the
294 steady-state abundance of genes [24-26]. A previously published method, SLAM-ITseq, extended
295 SLAM-seq to mouse tissues by crossing Cre-dependent UPRT mice with Cre lines [27]. This
296 method requires usage of transgenic animals, and the cell types that can be investigated are
297 restricted by available Cre lines. Instead of intravenously injecting 4-thiouracil and relying on Cre-
298 dependent UPRT expression for cell-specific labeling, we used stereotactic 4sU injection to target
299 all cell types in selected brain regions. Our data showed that 4sU can be effectively imported into
300 major cell types [28], and incorporated into the transcription, without causing detectable tissue
301 damage or cell death. This is a simplified method that can be applied to any brain region in mice
302 and possibly other species using stereotaxic injection, without the need for transgenic animals.
303
304 We used this method to investigate the RNA dynamics of a key brain region involved in stress
305 conditions, the amygdala, under acute and chronic restraint stress. We found partial overlap in
306 genes detected by SLAM-seq and RNA-seq, and over half of the overlapped up-regulated genes
307 under CS condition had been implicated in chronic stress by previous studies [52-54, 61-64].
308 Notably, for all these genes, SLAM-seq showed higher sensitivity than RNA-seq, shown by higher

fold changes and significance levels. The upregulated genes with high abundance were detected by SLAM-seq with high significance level, while barely meets the lenient criteria in RNA-seq. It supports the notion that for genes with high expression rate, physiological condition (restraint stress) may not cause a noticeable change in the total amount of mRNA for relevant genes. One such example is the ensemble of genes related to myelination. The high abundance of these genes precluded detection by RNA-seq following CS treatment, although immunostaining of myelin-specific protein revealed increased myelination, consistent with the SLAM-seq results. Therefore, SLAM-seq serves as a better method for screening the dynamics of highly expressed genes.

Competition and cooperation between excitation and inhibition is crucial for balancing neural activity[65, 66]. Using SLAM-seq, we identified 6 GABA receptors under AS, compared to 1 under BL and 4 under CS, suggesting an imminent inhibition drive induced by AS. Conversely, 3 glutamate receptors were identified under CS, while only 1 under AS and 0 under BL, suggesting an increase in elevated activity of the amygdala. Furthermore, CS also induced transcription of many genes associated with myelination. Myelination has been shown to be initiated by neuronal activities [20, 21], and can in turn facilitate signal transduction in neurons [51, 67]. These results are consistent with previous findings that stress could cause hyperactivity of the amygdala [14, 68, 69]. Therefore, our findings indicated that acute and chronic stress could differentially modulate the transcription level of GABA and glutamate receptors as well as proteins constituting the myelin sheath, and in turn influence the excitation-inhibition balance of the amygdala neurons.

We provided a rich dataset of molecular responses of amygdala to acute and chronic stress, and confirmed that CS can induce increased myelination through immunostaining. Future studies will be essential for understanding the functions of other genes identified in this study.

Acknowledgements

We thank Drs. Margaret Ho and Dan-Qian Liu for comments on the manuscript. We thank Dr. Hao Wu and Ms. Liang He for assistance in data analysis and experiments. We thank the animal facility of ShanghaiTech for their excellent care of mice. This work was supported by grants from the Ministry of Science and Technology of China (2022ZD0204900), Central Guidance on Local

Science and Technology Development Fund (YDZX20233100001002), and ShanghaiTech University Startup Fund to Y.Y.

References

1. Caspi, A., et al., Influence of life stress on depression: moderation by a polymorphism in the 5-HTT gene. Science, 2003. 301(5631): p. 386-9.
2. Weger, M. and C. Sandi, High anxiety trait: A vulnerable phenotype for stress-induced depression. Neurosci Biobehav Rev, 2018. 87: p. 27-37.
3. de Kloet, E.R., M. Joëls, and F. Holsboer, Stress and the brain: from adaptation to disease. Nat Rev Neurosci, 2005. 6(6): p. 463-75.
4. McEwen, B.S., Physiology and neurobiology of stress and adaptation: central role of the brain. Physiol Rev, 2007. 87(3): p. 873-904.
5. Xiao, Q., et al., A new GABAergic somatostatin projection from the BNST onto accumbal parvalbumin neurons controls anxiety. Mol Psychiatry, 2021. 26(9): p. 4719-4741.
6. Davis, M., et al., Phasic vs sustained fear in rats and humans: role of the extended amygdala in fear vs anxiety. Neuropsychopharmacology, 2010. 35(1): p. 105-35.
7. Mah, L., C. Szabuniewicz, and A.J. Fiocco, Can anxiety damage the brain? Curr Opin Psychiatry, 2016. 29(1): p. 56-63.
8. Liu, W.Z., et al., Identification of a prefrontal cortex-to-amygdala pathway for chronic stress-induced anxiety. Nat Commun, 2020. 11(1): p. 2221.
9. Liu, T., et al., Stress induces microglia-associated synaptic circuit alterations in the dorsomedial prefrontal cortex. Neurobiol Stress, 2021. 15: p. 100342.
10. Roozendaal, B., B.S. McEwen, and S. Chattarji, Stress, memory and the amygdala. Nat Rev Neurosci, 2009. 10(6): p. 423-33.
11. Zhang, J.Y., et al., Chronic Stress Remodels Synapses in an Amygdala Circuit-Specific Manner. Biol Psychiatry, 2019. 85(3): p. 189-201.
12. Quirk, G.J. and D.R. Gehlert, Inhibition of the amygdala: key to pathological states? Ann N Y Acad Sci, 2003. 985: p. 263-72.
13. Liu, Z.P., et al., Chronic stress impairs GABAergic control of amygdala through suppressing the tonic GABAA receptor currents. Mol Brain, 2014. 7: p. 32.
14. Zhang, X., et al., Stress-Induced Functional Alterations in Amygdala: Implications for Neuropsychiatric Diseases. Front Neurosci, 2018. 12: p. 367.
15. Herdegen, T. and J.D. Leah, Inducible and constitutive transcription factors in the mammalian nervous system: control of gene expression by Jun, Fos and Krox, and CREB/ATF proteins. Brain Res Brain Res Rev, 1998. 28(3): p. 370-490.
16. O'Donovan, K.J., et al., The EGR family of transcription-regulatory factors: progress at the interface of molecular and systems neuroscience. Trends Neurosci, 1999. 22(4): p. 167-73.
17. West, A.E. and M.E. Greenberg, Neuronal activity-regulated gene transcription in synapse development and cognitive function. Cold Spring Harb Perspect Biol, 2011. 3(6).
18. Gallo, F.T., et al., Immediate Early Genes, Memory and Psychiatric Disorders: Focus on c-Fos, Egr1 and Arc. Front Behav Neurosci, 2018. 12: p. 79.
19. Yap, E.L. and M.E. Greenberg, Activity-Regulated Transcription: Bridging the Gap between Neural Activity and Behavior. Neuron, 2018. 100(2): p. 330-348.
20. Mount, C.W. and M. Monje, Wrapped to Adapt: Experience-Dependent Myelination. Neuron, 2017. 95(4): p. 743-756.
21. Fields, R.D., A new mechanism of nervous system plasticity: activity-dependent myelination. Nat Rev Neurosci, 2015. 16(12): p. 756-67.
22. Lee, P.R. and R.D. Fields, Activity-Dependent Gene Expression in Neurons. Neuroscientist, 2021. 27(4): p. 355-366.

387 23. Herzog, V.A., et al., Thiol-linked alkylation of RNA to assess expression dynamics. Nat
388 Methods, 2017. 14(12): p. 1198-1204.
389 24. Alalam, H., J.A. Zepeda-Martinez, and P. Sunnerhagen, Global SLAM-seq for accurate
390 mRNA decay determination and identification of NMD targets. RNA, 2022. 28(6): p. 905-915.
391 25. Muhar, M., et al., SLAM-seq defines direct gene-regulatory functions of the BRD4-MYC
392 axis. Science, 2018. 360(6390): p. 800-805.
393 26. Bhat, P., et al., SLAMseq resolves the kinetics of maternal and zygotic gene expression
394 during early zebrafish embryogenesis. Cell Rep, 2023. 42(2): p. 112070.
395 27. Matsushima, W., et al., SLAM-ITseq: sequencing cell type-specific transcriptomes without
396 cell sorting. Development, 2018. 145(13).
397 28. Yao, S.Y., et al., Nucleobase transport by human equilibrative nucleoside transporter 1
398 (hENT1). J Biol Chem, 2011. 286(37): p. 32552-62.
399 29. Radle, B., et al., Metabolic labeling of newly transcribed RNA for high resolution gene
400 expression profiling of RNA synthesis, processing and decay in cell culture. J Vis Exp, 2013(78).
401 30. Gorczyca, W., et al., Presence of DNA strand breaks and increased sensitivity of DNA in
402 situ to denaturation in abnormal human sperm cells: analogy to apoptosis of somatic cells. Exp
403 Cell Res, 1993. 207(1): p. 202-5.
404 31. Neumann, T., et al., Quantification of experimentally induced nucleotide conversions in
405 high-throughput sequencing datasets. BMC Bioinformatics, 2019. 20(1): p. 258.
406 32. Goaillard, J.M. and E. Marder, Ion Channel Degeneracy, Variability, and Covariation in
407 Neuron and Circuit Resilience. Annu Rev Neurosci, 2021. 44: p. 335-357.
408 33. Hochgerner, H., et al., Neuronal types in the mouse amygdala and their transcriptional
409 response to fear conditioning. Nat Neurosci, 2023. 26(12): p. 2237-2249.
410 34. Yao, Z., et al., A high-resolution transcriptomic and spatial atlas of cell types in the whole
411 mouse brain. Nature, 2023. 624(7991): p. 317-332.
412 35. Li, S., et al., Effects of acute restraint stress on different components of memory as assessed
413 by object-recognition and object-location tasks in mice. Behav Brain Res, 2012. 227(1): p. 199-
414 207.
415 36. Love, M.I., W. Huber, and S. Anders, Moderated estimation of fold change and dispersion
416 for RNA-seq data with DESeq2. Genome Biol, 2014. 15(12): p. 550.
417 37. Baldelli, P., et al., Lack of synapsin I reduces the readily releasable pool of synaptic vesicles
418 at central inhibitory synapses. J Neurosci, 2007. 27(49): p. 13520-31.
419 38. Trapani, J.G., et al., Synaptojanin1 is required for temporal fidelity of synaptic transmission
420 in hair cells. PLoS Genet, 2009. 5(5): p. e1000480.
421 39. Montesinos, M.S., et al., Presynaptic Deletion of GIT Proteins Results in Increased
422 Synaptic Strength at a Mammalian Central Synapse. Neuron, 2015. 88(5): p. 918-925.
423 40. Jurado, S., et al., LTP requires a unique postsynaptic SNARE fusion machinery. Neuron,
424 2013. 77(3): p. 542-58.
425 41. Irfan, M., et al., SNAP-25 isoforms differentially regulate synaptic transmission and long-
426 term synaptic plasticity at central synapses. Sci Rep, 2019. 9(1): p. 6403.
427 42. Bozdagi, O., et al., The neurotrophin-inducible gene Vgf regulates hippocampal function
428 and behavior through a brain-derived neurotrophic factor-dependent mechanism. J Neurosci, 2008.
429 28(39): p. 9857-69.
430 43. Andolina, D., et al., Prefrontal/amygdalar system determines stress coping behavior
431 through 5-HT/GABA connection. Neuropsychopharmacology, 2013. 38(10): p. 2057-67.

44. Flati, T., et al., A gene expression atlas for different kinds of stress in the mouse brain. Sci Data, 2020. 7(1): p. 437.
45. Kolbasi, B., et al., Chronic unpredictable stress disturbs the blood-testis barrier affecting sperm parameters in mice. Reprod Biomed Online, 2021. 42(5): p. 983-995.
46. Asraf, K., et al., Synergistic, long-term effects of glutamate dehydrogenase 1 deficiency and mild stress on cognitive function and mPFC gene and miRNA expression. Transl Psychiatry, 2023. 13(1): p. 248.
47. Muller, H.K., et al., Differential expression of synaptic proteins after chronic restraint stress in rat prefrontal cortex and hippocampus. Brain Res, 2011. 1385: p. 26-37.
48. McEwen, B.S., Neurobiological and Systemic Effects of Chronic Stress. Chronic Stress (Thousand Oaks), 2017. 1.
49. Mozhui, K., et al., Strain differences in stress responsivity are associated with divergent amygdala gene expression and glutamate-mediated neuronal excitability. J Neurosci, 2010. 30(15): p. 5357-67.
50. Chen, C.C., et al., Selective activation of parvalbumin interneurons prevents stress-induced synapse loss and perceptual defects. Mol Psychiatry, 2018. 23(7): p. 1614-1625.
51. Stadelmann, C., et al., Myelin in the Central Nervous System: Structure, Function, and Pathology. Physiol Rev, 2019. 99(3): p. 1381-1431.
52. Gautam, A., et al., Acute and chronic plasma metabolomic and liver transcriptomic stress effects in a mouse model with features of post-traumatic stress disorder. PLoS One, 2015. 10(1): p. e0117092.
53. Kuehner, J.N., et al., Social defeat stress induces genome-wide 5mC and 5hmC alterations in the mouse brain. G3 (Bethesda), 2023. 13(8).
54. Mingardi, J., et al., Involvement of miR-135a-5p Downregulation in Acute and Chronic Stress Response in the Prefrontal Cortex of Rats. Int J Mol Sci, 2023. 24(2).
55. Kosuth, J., et al., Selection of Reliable Reference Genes for Analysis of Gene Expression in Spinal Cord during Rat Postnatal Development and after Injury. Brain Sci, 2019. 10(1).
56. Pelkey, K.A., et al., Pentraxins Coordinate Excitatory Synapse Maturation and Circuit Integration of Parvalbumin Interneurons. Neuron, 2016. 90(3): p. 661.
57. Fan, R. and K.O. Lai, Understanding how kinesin motor proteins regulate postsynaptic function in neuron. FEBS J, 2022. 289(8): p. 2128-2144.
58. Gerfen, C.R. and P.E. Sawchenko, An anterograde neuroanatomical tracing method that shows the detailed morphology of neurons, their axons and terminals: immunohistochemical localization of an axonally transported plant lectin, Phaseolus vulgaris leucoagglutinin (PHA-L). Brain Res, 1984. 290(2): p. 219-38.
59. Frey, U. and R.G. Morris, Synaptic tagging and long-term potentiation. Nature, 1997. 385(6616): p. 533-6.
60. Rangaraju, V., S. Tom Dieck, and E.M. Schuman, Local translation in neuronal compartments: how local is local? EMBO Rep, 2017. 18(5): p. 693-711.
61. Issler, O., et al., MicroRNA 135 is essential for chronic stress resiliency, antidepressant efficacy, and intact serotonergic activity. Neuron, 2014. 83(2): p. 344-360.
62. Jaffe, A.E., et al., Decoding Shared Versus Divergent Transcriptomic Signatures Across Cortico-Amygdala Circuitry in PTSD and Depressive Disorders. Am J Psychiatry, 2022. 179(9): p. 673-686.
63. Ochi, S. and Y. Dwivedi, Dissecting early life stress-induced adolescent depression through epigenomic approach. Mol Psychiatry, 2023. 28(1): p. 141-153.

478 64. McMurray, K.M.J., et al., Identification of a novel, fast-acting GABAergic antidepressant.
479 Mol Psychiatry, 2018. 23(2): p. 384-391.
480 65. Bhatia, A., S. Moza, and U.S. Bhalla, Precise excitation-inhibition balance controls gain
481 and timing in the hippocampus. Elife, 2019. 8.
482 66. Wang, X., et al., Metabolic tuning of inhibition regulates hippocampal neurogenesis in the
483 adult brain. Proc Natl Acad Sci U S A, 2020. 117(41): p. 25818-25829.
484 67. Suminaite, D., D.A. Lyons, and M.R. Livesey, Myelinated axon physiology and regulation
485 of neural circuit function. Glia, 2019. 67(11): p. 2050-2062.
486 68. Pitman, R.K., et al., Biological studies of post-traumatic stress disorder. Nat Rev Neurosci,
487 2012. 13(11): p. 769-87.
488 69. Roozendaal, B., J.M. Koolhaas, and B. Bohus, The role of the central amygdala in stress
489 and adaption. Acta Physiol Scand Suppl, 1997. 640: p. 51-4.
490
491

492 **Figure legends**

493 **Fig. 1：SLAM-seq for mouse brain cells by stereotactic injection of 4sU into the brain.**

494 **(a)** Schematic showing SLAM-seq procedure, including stereotactic 4sU injection, RNA
495 extraction, iodoacetamide (IAA) treatment, RNA sequencing and T-C conversion detection.

496 **(b)** Dot blot essay of RNA extracted from mouse brain labeled with 4sU for different durations.
497 Left to right: biotin-oligo (positive control); RNA samples extracted from mouse auditory
498 cortex with no 4sU injection (negative control); 2 h, 8 h, and 24 h after 4sU injection.

499 **(c)** TUNEL staining of brain slices for positive control (top panels), and brain slices with DMSO
500 (middle) and 4sU (bottom) injections in auditory cortex. Green signals denoted dead cells.
501 Scale bar, 50 μm.

502 **(d)** Correlation of RNA levels extracted from DMSO (denoted as 4sU-) and 4sU (denoted as 4sU+)
503 injected auditory cortex samples. ρ, spearman correlation coefficient.

504

505 **Fig. 2：Identifying 4sU-labeled genes with SLAM-seq and match to different cell types**

506 **(a)** Time line showing stereotactic 4sU injection and brain extraction under baseline (BL)
507 condition. Shading demonstrates nascent mRNA that can be detected by SLAM-seq.

508 **(b)** T>C Conversion rates of total mRNA extracted from DMSO (n=5) and 4sU (n=4) injected
509 amygdala under baseline condition.

510 **(c)** Volcano plots showing T>C conversion rates of transcripts under baseline, with or without
511 4sU injection. Red dots represent transcripts with significant higher T>C conversion rates in
512 the 4sU+ group (FDR < 0.05 and $\log_2$FC > 1); blue dots represent transcripts with significant
513 lower T>C conversion rates in the 4sU+ group (FDR < 0.05 and $\log_2$FC < -1).

514 **(d)** T>C Conversion rates of marker genes for multiple neuron and glia cell types.

515

516 **Fig. 3：Transcriptome dynamics of mouse amygdala under acute stress.**

517 **(a)** Time line of acute stress experiment, including time points for 4sU injection and brain
518 extraction.

519 **(b)** Volcano plots showing T>C conversion rates of transcripts under AS, with or without 4sU
520 injection. Red dots represent transcripts with significant higher T>C conversion rates in the
521 4sU+ group (FDR < 0.05 and $\log_2$FC > 1); blue dots represent transcripts with significant lower
522 T>C conversion rates in the 4sU+ group (FDR < 0.05 and $\log_2$FC < -1).

523 **(c)** GO term analysis for genes detected by SLAM-seq.

524 **(d)** KEGG analysis for genes detected by SLAM-seq.

525 **(e)** Fold changes of T>C conversion rates for GABA and glutamate receptors detected by SLAM-
526 seq. Student's t-test, *** $P < 0.001$.

527 **(f)** Volcano plots showing differentially expressed genes (DEGs) under AS compared to BL. Red
528 dots represent significantly AS-upregulated genes (FDR < 0.1 and $\log_2FC > 0.1$); blue dots
529 represent significantly AS-downregulated genes (FDR<0.1 and $\log_2FC < -0.1$). ns, no
530 significant difference; up, significantly upregulated; down, significantly downregulated.

531 **(g)** Venn diagram showing intersection of AS-specific genes identified by SLAM-seq (red dots in
532 **b**) and RNA-seq (red dots in **f**).

533 **(h)** Fold changes of T>C conversion rates for 4sU+ vs. 4sU- (SLAM), and of expression levels for
534 AS vs. BL (DEG) of all overlapped genes in (**g**). Paired t-test, *** $P < 0.001$.

535 **(i)** Correlation between FC-DEG and expression levels of AS-upregulated genes in **3g**, with the
536 color and size of each data point denoting the significance level (FDR-SLAM) and fold change
537 (FC-SLAM) of each AS-upregulated gene.

538 **(j)** Distribution for expression levels of genes detected by SLAM-seq and RNA-seq under AS.
539 Two-sample Kolmogorov-Smirnov test, $p < 0.05$

540 **(k)** Significance levels of T>C conversion rates for 4sU+ vs. 4sU- (SLAM), and of expression
541 levels for AS vs. BL (DEG) of all overlapped genes in (**g**). Paired t-test, *** $P < 0.001$.

542

543 **Fig. 4：Transcriptome dynamics of mouse amygdala under chronic stress.**

544 **(a)** Time line of chronic stress experiment, including time points for 4sU injection and brain
545 extraction.

546 **(b)** Volcano plots showing T>C conversion rates of transcripts under CS, with or without 4sU
547 injection. Red dots represent transcripts with significant higher T>C conversion rates in the
548 4sU+ group (FDR < 0.05 and $\log_2FC > 1$); blue dots represent transcripts with significant lower
549 T>C conversion rates in the 4sU+ group (FDR < 0.05 and $\log_2FC < -1$).

550 **(c)** GO term analysis for genes detected by SLAM-seq.

551 **(d)** Volcano plots showing differentially expressed genes (DEGs) under CS compared to BL. Red
552 dots represent significantly AS-upregulated genes (FDR < 0.1 and $\log_2FC > 0.1$); blue dots
553 represent significantly AS-downregulated genes (FDR<0.1 and $\log_2FC < -0.1$).

554 **(e)** Venn diagram showing intersection of AS-specific genes identified by SLAM-seq (red dots in
555 **b**) and RNA-seq (red dots in **d**).
556 **(f)** Correlation between FC-DEG and expression levels of AS-upregulated genes in **e**, with the
557 color and size of each data point denoting the significance level (FDR-SLAM) and fold change
558 (FC-SLAM) of each CS-upregulated gene.
559 **(g)** Distribution for expression levels of genes detected by SLAM-seq and RNA-seq under CS.
560 Two-sample Kolmogorov-Smirnov test, $p < 0.05$.
561 **(h)** Fold changes of T>C conversion rates for 4sU+ vs. 4sU- (SLAM), and of expression levels for
562 AS vs. BL (DEG) of all overlapped genes in (**e**). Paired t-test, *** $P < 0.001$.
563 **(i)** Significance levels of T>C conversion rates for 4sU+ vs. 4sU- (SLAM), and of expression
564 levels for AS vs. BL (DEG) of all overlapped genes in (**e**). Paired t-test, * $P < 0.05$.
565
566 **Fig. 5: Comparison of AS and CS-associated genes and validation of SLAM-seq results**
567 **(a)** Venn diagram showing intersections of genes identified by SLAM-seq under BL, AS and CS
568 conditions. Genes associated with synapse, postsynaptic plasticity, autophagy and myelination
569 are listed.
570 **(b)** GO term analysis for AS-specific genes detected by SLAM-seq.
571 **(c)** Fold changes of T>C conversion rates for GABA and glutamate receptors detected by SLAM-
572 seq under CS. Student's t-test, *** $P < 0.001$.
573 **(d)** Fold changes of T>C conversion rates for myelination related genes detected by SLAM-seq
574 under CS. Student's t-test, *** $P < 0.001$.
575 **(e)** GO term analysis for CS-specific genes detected by SLAM-seq.
576 **(f)** Example images showing immunostaining of myelin basic protein (MBP) in the amygdala of
577 control (BL) and chronically stressed (CS) mice. Scale bar, 20 μm.
578 **(g)** Increased MBP signal intensity in CS mice (n=5) compared to BL mice (n=5), measured by
579 mean gray value. Student's t-test, ** $p<0.01$.
580
581

582 **Materials and methods**

583 **Animals**

584 C57BL/6 mice were purchased from Slac Laboratory Animals. Mice were housed and bred in a 12
585 h light-dark cycle (7 am - 7 pm light) in the animal facility of ShanghaiTech University. Eight- to
586 ten-week-old male mice were used for the experiments. All procedures were approved by the
587 Animal Committee of ShanghaiTech University.

588

589 **4sU Injection**

590 The 4sU powder was dissolved in dimethyl sulfoxide (DMSO) to reach a concentration of 1 M,
591 and the solution was aliquoted, frozen, and stored at -20°C. Before injection, the solution was 1:10
592 diluted with phosphate-buffered saline (PBS). For injection, mice were anesthetized with
593 isoflurane (1.5-2 %) and positioned in a stereotaxic frame (RWD Life Science Co.). Body
594 temperature was maintained at 37 °C using a heating pad. 4sU solution (1 μL) were injected using
595 a glass micropipette with a tip diameter of 15–20 μm, through a small skull opening (<0.5 mm2),
596 with a microinjector (Nanoject III), at a rate of 1 nL/s. In baseline, acute stress and chronic stress
597 experiments, 4sU was injected into bilateral amygdala 24 h before brain extraction.

598

599 **TUNEL Staining**

600 The TUNEL assay was performed following the one-step method outlined in the Promega TUNEL
601 Cell Apoptosis Detection Kit. Mice were intracranially injected with 1 μL of 100 mM 4sU into the
602 auditory cortex (M/L=-4.4 mm, A/P=-2.2 mm, D/V=-1.1 mm) or amygdala (M/L=±3.25 mm,
603 A/P=-1.1 mm, D/V=-3.95 mm), as described above. After 24 h, mice were deeply anesthetized and
604 transcardially perfused with PBS and paraformaldehyde (PFA), followed by brain extraction. The
605 extracted brains were postfixed in PFA at 4°C for 12 hours and embedded in agarose for vibratome
606 sectioning at 70 μm per slice. Brain slices were collected for TUNEL staining, in which terminal
607 deoxynucleotidyl transferase (TdT) labels DNA strand breaks with fluorophore-labeled
608 nucleotides. Stained brain slices were mounted on glass slides and imaged using confocal
609 fluorescence microscopy (Leica).

610

611 **Tissue RNA Extraction**

612 Mice were deeply anesthetized and transcardially perfused with cold PBS. Each mouse was then
613 quickly decapitated, and the head was immersed in ice-cold PBS for rapid cooling for 10 seconds.
614 The mouse brain was then carefully extracted using forceps, placed in a pre-chilled mouse brain
615 mold (RWD Life Science Inc.), and a 2 mm-thick brain tissue block containing the target region
616 (auditory cortex or amygdala) was sliced using a razor blade. The brain slice was then placed on a
617 6 mm petri dish and dropped into liquid nitrogen briefly for 7-8 s. Then, the auditory cortex or
618 amygdala was cut out using a 15 G needle, and promptly transferred to cryotubes for rapid freezing
619 in liquid nitrogen, and subsequent storage at -80°C.
620
621 RNA extraction from mouse brain tissue was performed using the Trizol method. The frozen tissue
622 in cryotubes was thawed, and 1 mL of Trizol (MagZol Reagent R4801-02) was added to each tube.
623 Tissue homogenization was performed using an electric homogenizer, with a 10-second pause
624 every 10 seconds to prevent overheating. The mixture was then left at room temperature for 5
625 minutes for tissue digestion, and the liquid was transferred to 1.5 mL centrifuge tubes. To each
626 tube, 200 μL of chloroform (one-fifth of the Trizol volume) was added, and after thorough vortex
627 mixing, the mixture was left at room temperature for 15 minutes. The mixture was then centrifuged
628 at 12,000 rpm for 15 minutes at 4°C. Then, the supernatant containing RNA was carefully aspirated
629 into new tubes, an equal volume of pre-cooled isopropanol was added, along with 1/100 volume
630 of 10 mM DTT (final concentration 0.1 mM) and 1 μL glycogen (20 mg/mL). After thorough
631 mixing, the mixture was left at -20°C for 1 hour for RNA precipitation. Subsequently, it was
632 centrifuged at 12,000 rpm for 30 minutes at 4°C, resulting in a white gel-like RNA substance at
633 the bottom. The RNA pellet was washed once with pre-cooled 75% ethanol (containing 5 μL 10
634 mM DTT), and after removing the supernatant, the RNA pellet was air-dried for approximately 3-
635 5 minutes. Finally, the RNA was dissolved in 20 μL RNase-free water, and the concentration was
636 determined using Nanodrop 2000.
637
638 **Dot Blot Assay**
639 Four RNA samples with different 4sU injection conditions were used in this experiment: 1) RNA
640 extracted from cortex with no 4sU injection, 2) RNA extracted from cortex dissected 2 h after 4sU
641 injection, 3) RNA extracted from cortex dissected 8 h after 4sU injection, 4) RNA extracted from
642 cortex dissected 24 h after 4sU injection. Positive control was 5′-biotin labeled DNA oligo.

643 Positive control and the extracted RNA samples (1 μg for each sample) were used for dot blot
644 essay following the standard protocol for Chemiluminescent Biotin-labeled Nucleic Acid
645 Detection Kit (Beyotime, D3308), using EZ-Link™ HPDP-Biotin (Thermo Scientific, 21341).
646
647 **Restraint Stress Experiment**
648 Mice were acclimated in the animal facility for at least one week before the initiation of restraint
649 stress experiments.
650 *Acute stress group:*
651 Each mouse was carefully removed from its home cage and put in a Falcon 50 mL centrifuge tube,
652 with 8 small ventilation holes drilled on the tube walls. Once the mouse entered the tube, the rear
653 was sealed with a clean tissue, and the tube was capped with the lid, preventing forward or
654 backward movements. Following the 1.5-hour restraint, the mouse was perfused and the brain was
655 extracted.
656 *Chronic stress group:*
657 Each mouse was carefully removed from its home cage and put in a 50 mL tube, as described in
658 the acute stress experiment. Daily restraint sessions lasting 2 hours (from 10:00 am to 12:00 pm)
659 were conducted for one week. On the 7th day, 10 hours after the final restraint session ended, the
660 mouse was perfused and the brain was extracted.
661 *Baseline group:*
662 Mice did not undergo any restraint stress, and remained in their home cages until they were
663 perfused.
664
665 **IAA treatment**
666 Extracted RNA was reacted with IAA to alkylate the thiol group following [1]. For a 50 μL reaction:
667 2-3 μg RNA, 25 μL DMSO, 5 μL 100 mM iodoacetamide (IAA), and 5 μL 500 mM sodium
668 phosphate (pH=8), and RNase-free water. IAA was freshly prepared and diluted with anhydrous
669 ethanol. The prepared mixture was incubated at 50°C for 15 minutes, followed by the addition of
670 1 M dithiothreitol (DTT) to terminate the reaction. Then, 125 μL anhydrous ethanol, 1 μL glycogen
671 (20 mg/mL), and 5 μL sodium acetate (3 M, pH=5.2) were added to the reaction system. After
672 thorough mixing, the solution was left at -80°C for 30 minutes, followed by centrifugation at
673 12,000 rpm for 30 minutes at 4°C, resulting in a white gel-like RNA substance at the bottom. The

674 RNA pellet was washed once with pre-cooled 75% ethanol. After removing the supernatant, the
675 RNA pellet was air-dried for approximately 3-5 minutes, and dissolved in 20 μL RNase-free water.
676
677 **RNA sequencing**
678 The IAA-methylated RNA was stored in a -80°C freezer, and library construction and sequencing
679 were conducted by Suzhou Geneseeq Technology Inc. The libraries were sequenced using the
680 Illumina NovaSeq for 150-base pair paired-end sequencing, generating approximately 6 GB of
681 sequencing data for each RNA sample.
682
683 **Bioinformatics Analysis**
684 *Preprocessing of RNA-Seq Data:*
685 Raw data obtained from RNA-Seq was preprocessed using Cutadapt v3.1. Adapter sequences in
686 paired-end sequencing were eliminated, and sequences shorter than 15 nucleotides were discarded.
687 The preprocessed data was then aligned to the NCBI reference mouse genome (mm10) using
688 Hisat2 v2.1.0. The resulting alignment data in SAM format was converted to BAM format using
689 Samtools v1.9.
690
691 *SLAM-Seq Analysis:*
692 The software SLAM-DUNK v0.2.4 (tneumann.github.io/slamdunk/), designed for SLAM-Seq
693 analysis, was used to compute the T>C mutation counts for each sample [2]. Annotation data for
694 3' UTR regions were obtained from the RefSeq and Ensembl databases. To identify significantly
695 4sU-labeled transcripts, a two-step filtering process was implemented. Firstly, genes with zero T
696 read counts were excluded. Secondly, only genes with read counts > 5 in all samples were kept for
697 further analyses. Statistical analysis was performed using the ibb R package (version 13.06), as
698 described in [3]. To control for the false discovery rate (FDR), adjusted P-values were calculated
699 using the Benjamini-Hochberg method. Transcripts with an FDR below 0.05 were considered
700 significantly labeled.
701
702 *Differential Gene Expression (DEG) Analysis:*
703 Quantification of gene expression was performed using FeatureCounts (v2.0.1). The Transcripts
704 Per Million (TPM) values for each gene were calculated using the formula:

705 $TPM = RPK / \sum RPK \times 10^6$

706 Here, RPK (Reads Per Kilobase) represents the reads per thousand base pairs, and ∑RPK is the
707 sum of RPK values for all genes in the sample. Differential expression analysis was performed
708 using the DESeq2 package in R 3.6.1. The standard DESeq2 workflow was followed for data
709 normalization, variance estimation, and statistical modeling. Identification of significantly
710 differentially expressed genes was based on the criterion of adjusted P-values < 0.05 or < 0.1.
711

712 **GO term enrichment analysis**

713 List of genes was used as input for PANTHER 13.1 (pantherdb.org/) to perform 'Statistical
714 enrichment test' with GO terms for biological processes, cellular components and molecular
715 functions. The enriched GO terms obtained were further selected based on the P-values for
716 visualization.
717

718 **Immunofluorescence**

719 Chronic stressed mice were perfused 2 weeks after the final restraint session ended, with 0.01M
720 PBS and 4% PFA. Control mice were perfused without any stress treatment. Brains were sliced (at
721 50 μm) using a vibratome (Leica VT1200S) after post-fixed for 5 d in 4% PFA at 4 °C. Brain slices
722 including the amygdala were permeabilized with 0.4% Triton X-100 in PBS for 30 minutes,
723 blocked with 5% bovine serum albumin (BSA) in PBS for 1 h at RT, and incubated with rat anti-
724 MBP (1:200; MCA409S, Serotec) in 0.1% Triton X-100 and 1% BSA in PBS for 40 h at 4°C, then
725 washed with PBS 3 × 10 minutes. Sections were incubated with DAPI (1:2500) and fluorophore-
726 conjugated secondary antibodies (1:500; AB150165, abcam) in 0.1% Triton X-100 and 1% BSA
727 in PBS for 2h at RT, then washed with PBS 3 × 10 minutes. Images were acquired at a Leica
728 STELLARIS 8 FALCON, with a HC FLUOTAR L VISIR 25x/0.95 water objective; pinhole was
729 set to 1 AU, pixel size to 113.55nm × 113.55nm and z-stack interval to 1 μm.
730 Image processing and quantification were performed using FIJI. For the quantitative
731 immunofluorescence analysis, the mean grey value of each field of view was first thresholded for
732 identification of myelin structures, and then calculated for 11 optical planes of acquired z-stacks
733 (step 1 μm). For each mouse, the mean grey value is averaged across two sections containing the
734 amygdala, one from each hemisphere.
735

References

1. Herzog, V.A., et al., *Thiol-linked alkylation of RNA to assess expression dynamics.* Nat Methods, 2017. **14**(12): p. 1198-1204.
2. Neumann, T., et al., *Quantification of experimentally induced nucleotide conversions in high-throughput sequencing datasets.* BMC Bioinformatics, 2019. **20**(1): p. 258.
3. Pham, T.V., et al., *On the beta-binomial model for analysis of spectral count data in label-free tandem mass spectrometry-based proteomics.* Bioinformatics, 2010. **26**(3): p. 363-9.

Figure 1

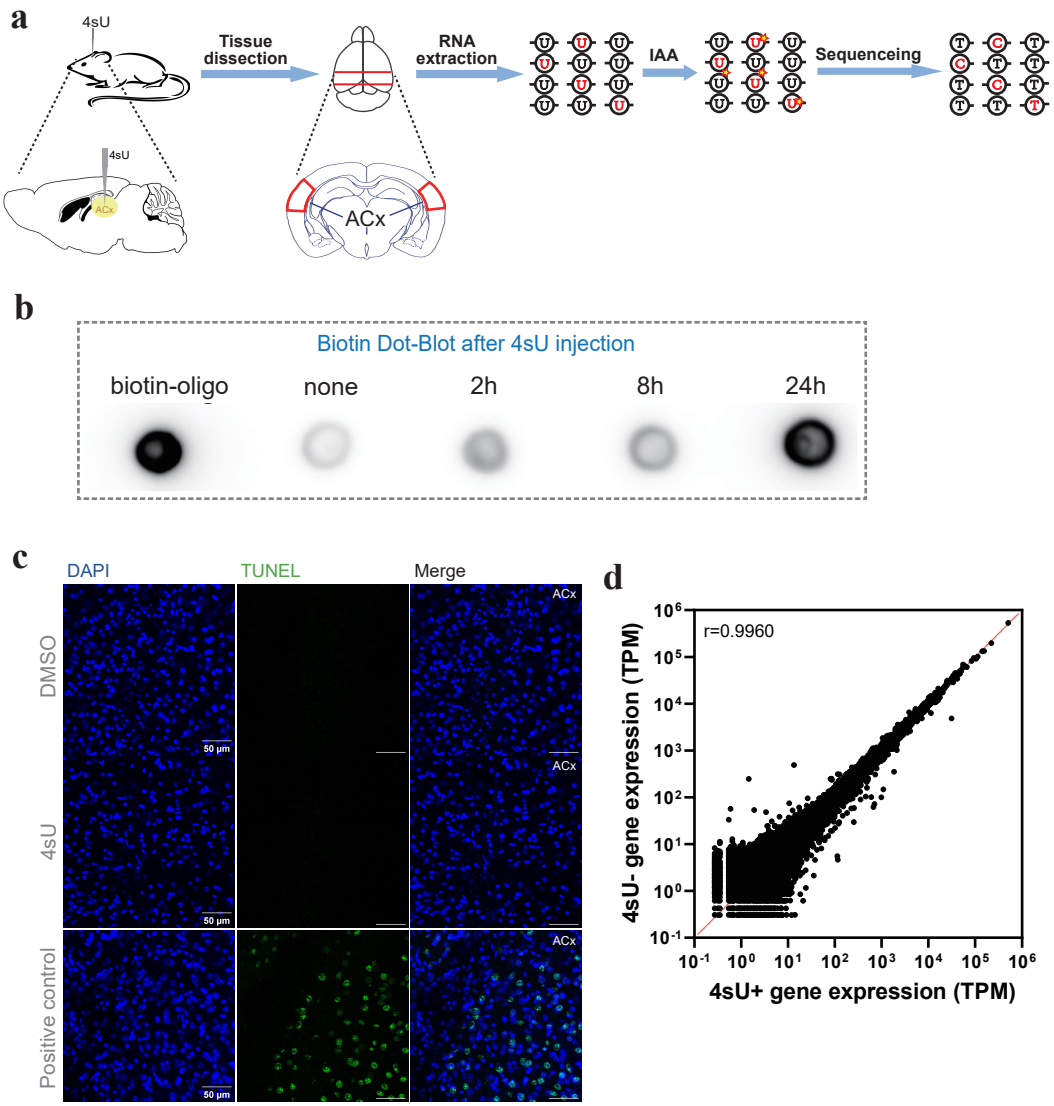
a
4sU
Tissue dissection
RNA extraction
IAA
Sequenceing
ACx
b
Biotin Dot-Blot after 4sU injection
biotin-oligo
none
2h
8h
24h
c
DAPI
TUNEL
Merge
DMSO
4sU
Positive control
ACx
50 μm
d
r=0.9960
4sU- gene expression (TPM)
4sU+ gene expression (TPM)

Figure 2

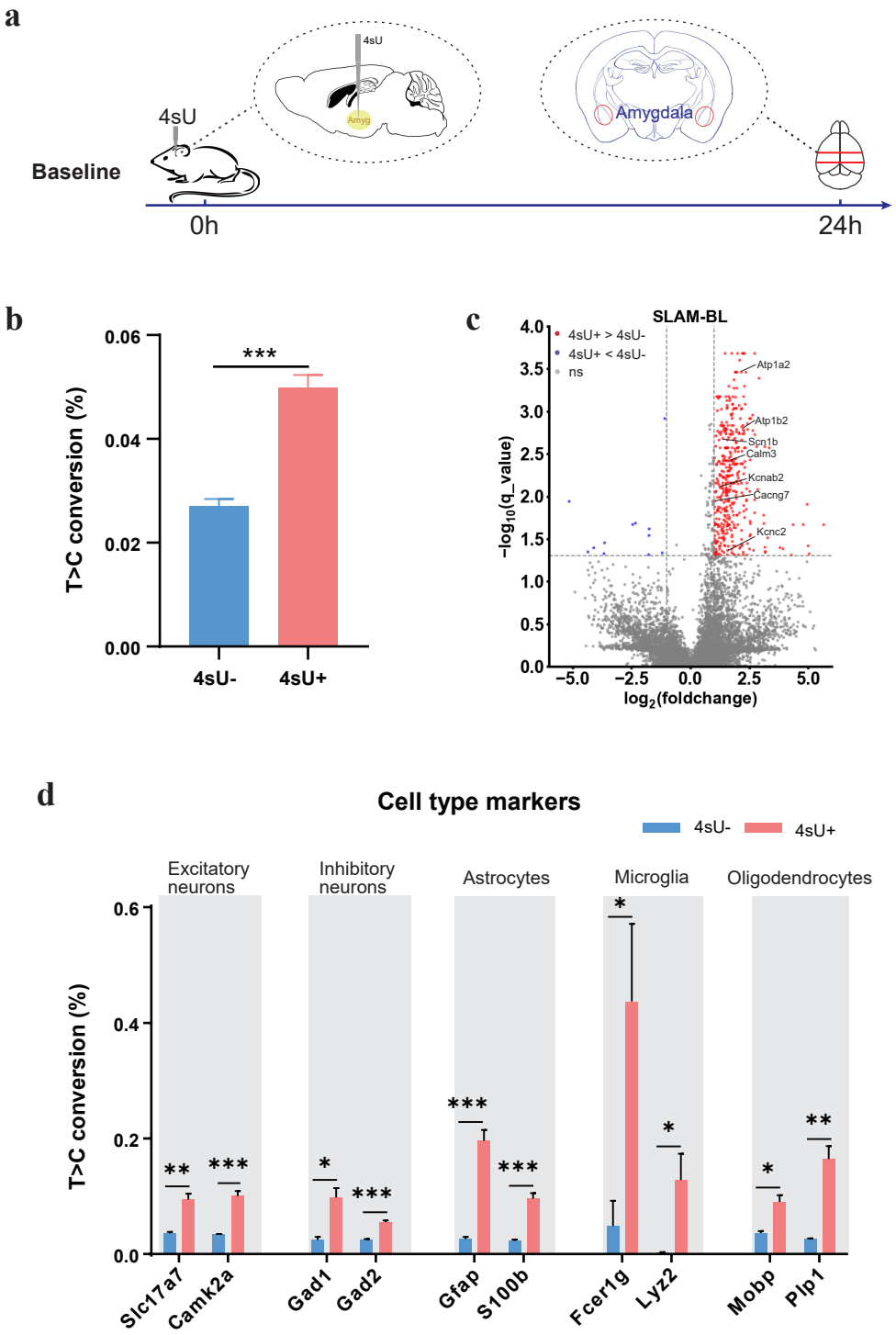
a
4sU
Baseline
4sU
Amyg
Amygdala
0h
24h
b
T>C conversion (%)
0.06
0.04
0.02
0.00
***
4sU-
4sU+
c
SLAM-BL
4sU+ > 4sU-
4sU+ < 4sU-
ns
Atp1a2
Atp1b2
Scn1b
Calm3
Kcnab2
Cacng7
Kcnc2
−log10(q_value)
log2(foldchange)
d
Cell type markers
4sU-
4sU+
Excitatory neurons
Inhibitory neurons
Astrocytes
Microglia
Oligodendrocytes
T>C conversion (%)
Slc17a7
Camk2a
Gad1
Gad2
Gfap
S100b
Fcer1g
Lyz2
Mobp
Plp1

Figure 3

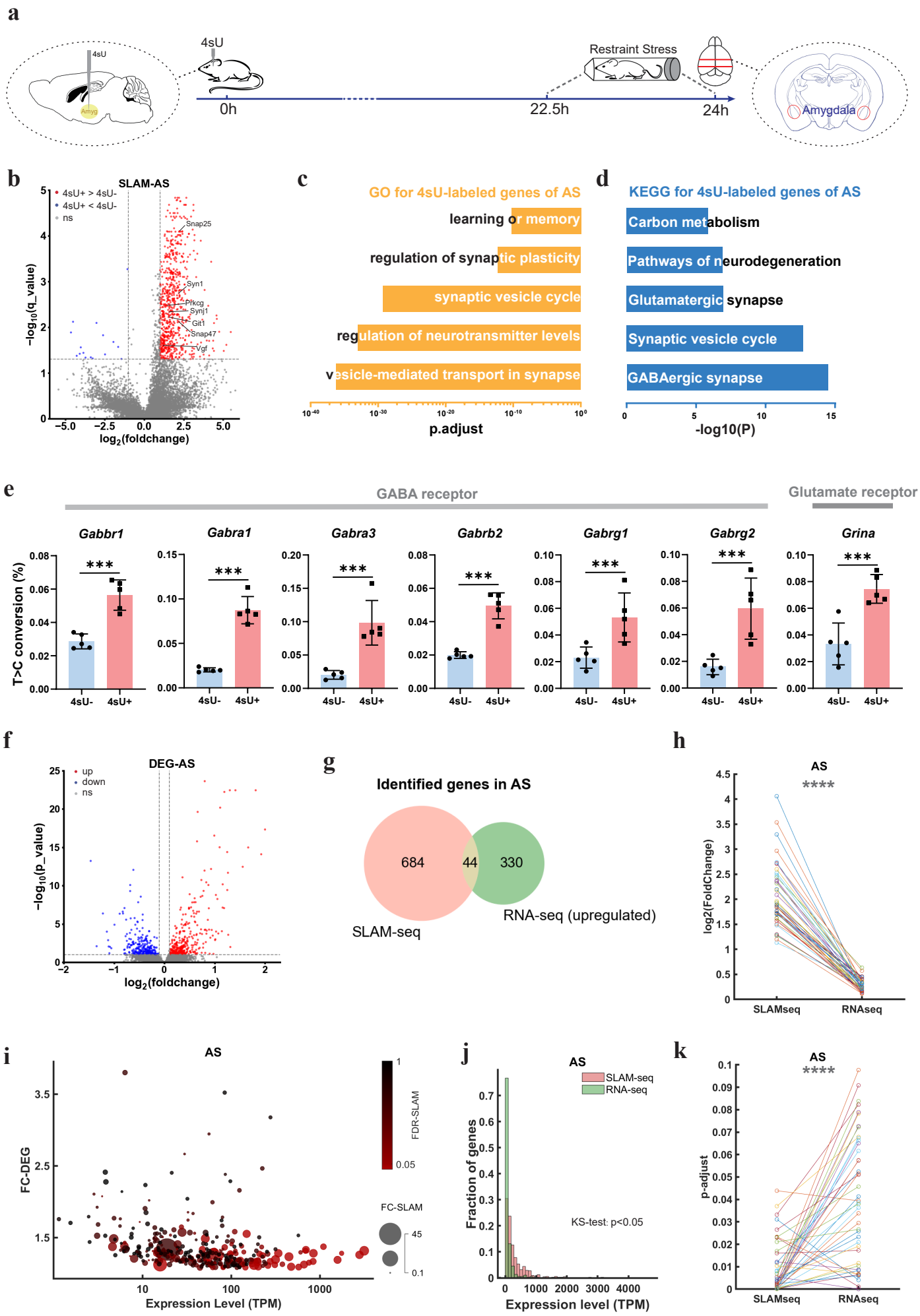
a
4sU
Amyg
4sU
0h
Restraint Stress
22.5h
24h
Amygdala
b
SLAM-AS
4sU+ > 4sU-
4sU+ < 4sU-
ns
Snap25
Syn1
Pfkcg
Synj1
Git1
Snap47
Vgf
−log10(q_value)
log2(foldchange)
c
GO for 4sU-labeled genes of AS
learning or memory
regulation of synaptic plasticity
synaptic vesicle cycle
regulation of neurotransmitter levels
vesicle-mediated transport in synapse
p.adjust
d
KEGG for 4sU-labeled genes of AS
Carbon metabolism
Pathways of neurodegeneration
Glutamatergic synapse
Synaptic vesicle cycle
GABAergic synapse
-log10(P)
e
GABA receptor
Glutamate receptor
Gabbr1
Gabra1
Gabra3
Gabrb2
Gabrg1
Gabrg2
Grina
T>C conversion (%)
4sU-
4sU+
f
DEG-AS
up
down
ns
−log10(p_value)
log2(foldchange)
g
Identified genes in AS
684
44
330
SLAM-seq
RNA-seq (upregulated)
h
AS
log2(FoldChange)
SLAMseq
RNAseq
i
AS
FC-DEG
Expression Level (TPM)
FDR-SLAM
FC-SLAM
j
AS
SLAM-seq
RNA-seq
Fraction of genes
KS-test: p<0.05
Expression level (TPM)
k
AS
p-adjust
SLAMseq
RNAseq

Figure 4

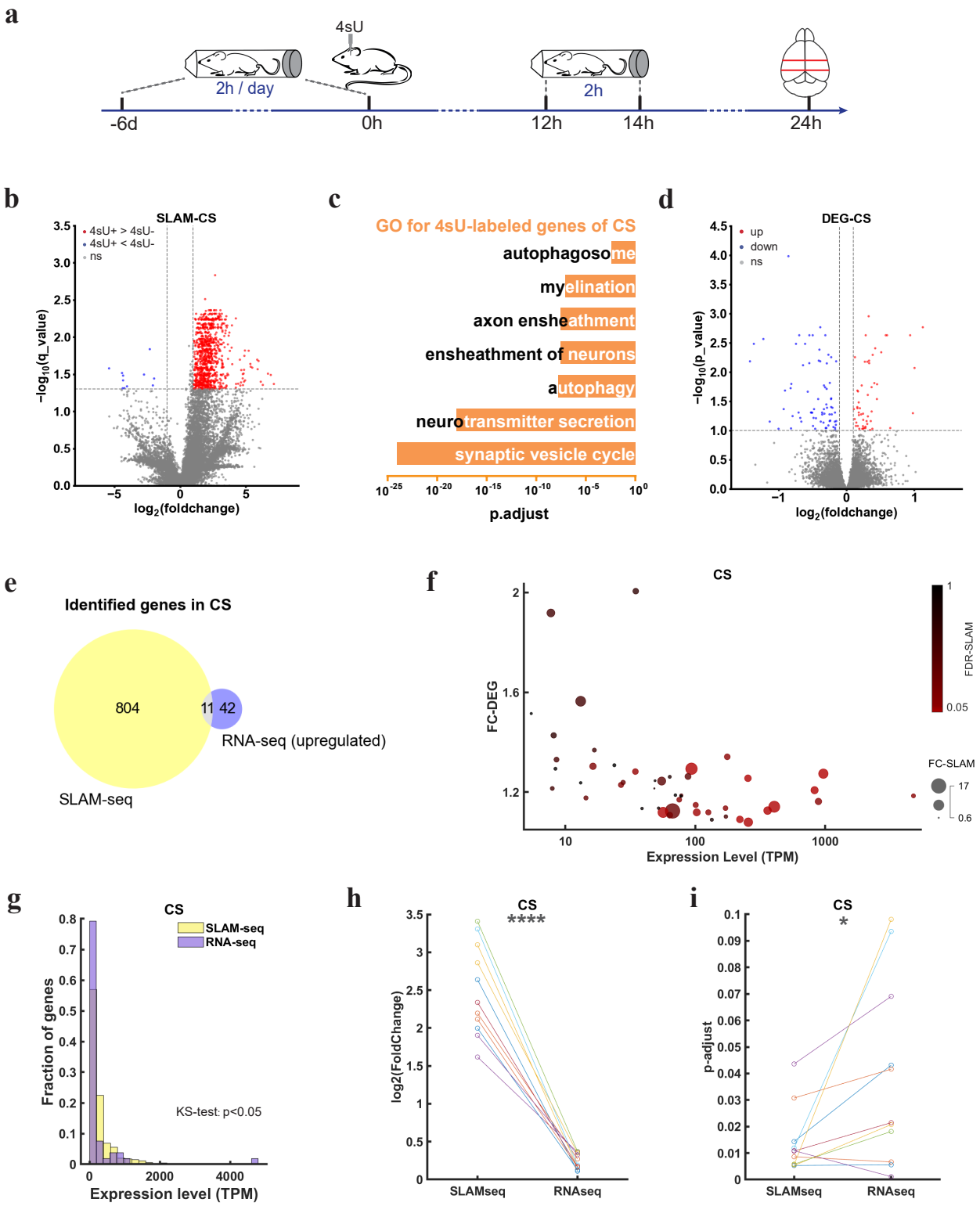
a
4sU
2h / day
2h
-6d
0h
12h
14h
24h
b
SLAM-CS
4sU+ > 4sU-
4sU+ < 4sU-
ns
−log10(q_value)
log2(foldchange)
c
GO for 4sU-labeled genes of CS
autophagosome
myelination
axon ensheathment
ensheathment of neurons
autophagy
neurotransmitter secretion
synaptic vesicle cycle
p.adjust
d
DEG-CS
up
down
ns
−log10(p_value)
log2(foldchange)
e
Identified genes in CS
804
11
42
RNA-seq (upregulated)
SLAM-seq
f
CS
FC-DEG
Expression Level (TPM)
FDR-SLAM
FC-SLAM
g
CS
SLAM-seq
RNA-seq
Fraction of genes
KS-test: p<0.05
Expression level (TPM)
h
CS
****
log2(FoldChange)
SLAMseq
RNAseq
i
CS
*
p-adjust
SLAMseq
RNAseq

Figure 5

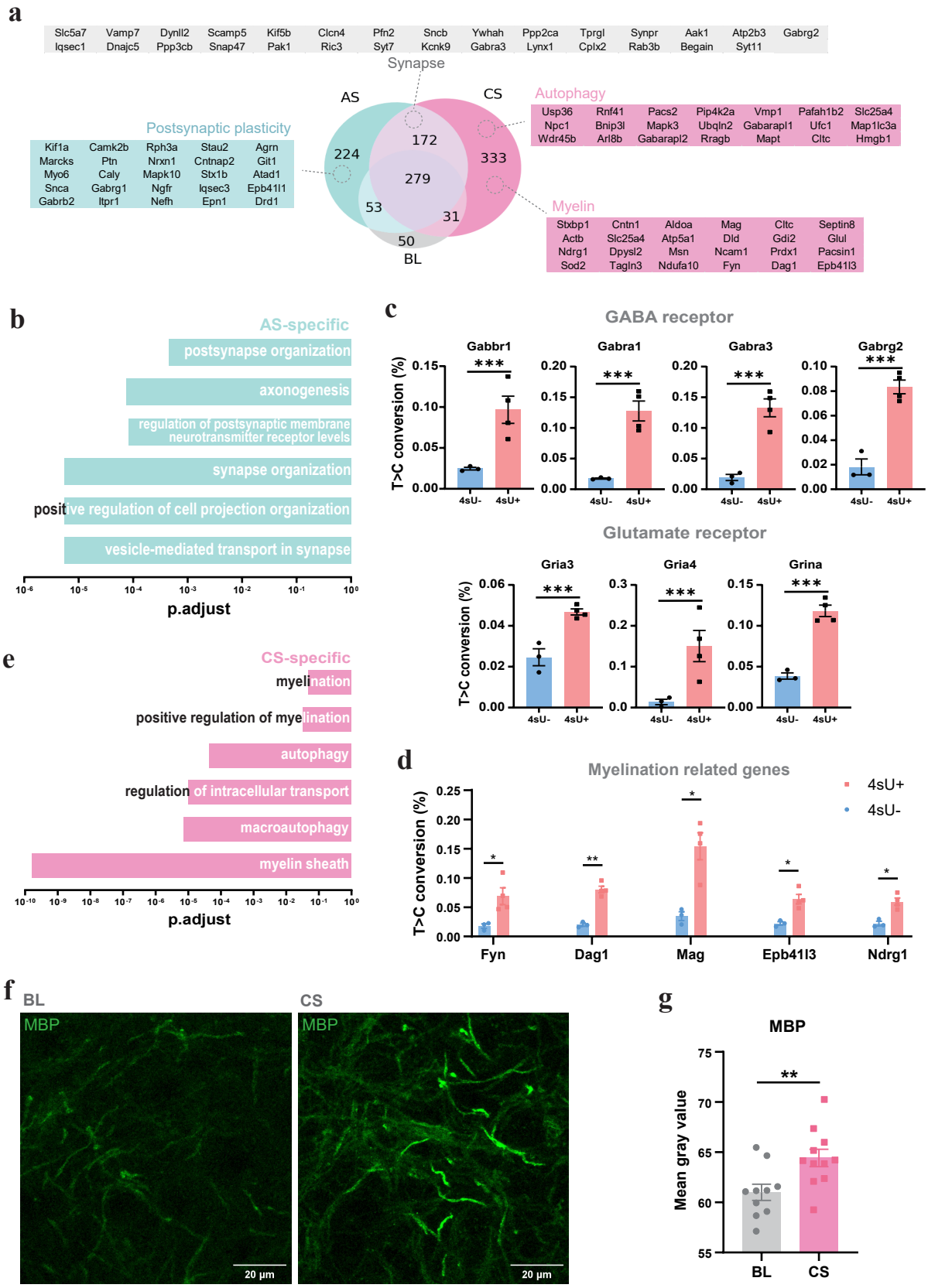
a
Slc5a7 Vamp7 DynII2 Scamp5 Kif5b Clcn4 Pfn2 Sncb Ywhah Ppp2ca Tprgl Synpr Aak1 Atp2b3 Gabrg2
Iqsec1 Dnajc5 Ppp3cb Snap47 Pak1 Ric3 Syt7 Kcnk9 Gabra3 Lynx1 Cplx2 Rab3b Begain Syt11
Synapse
AS
CS
BL
224
172
333
279
53
31
50
Postsynaptic plasticity
Kif1a Camk2b Rph3a Stau2 Agrn
Marcks Ptn Nrxn1 Cntnap2 Git1
Myo6 Caly Mapk10 Stx1b Atad1
Snca Gabrg1 Ngfr Iqsec3 Epb41l1
Gabrb2 Itpr1 Nefh Epn1 Drd1
Autophagy
Usp36 Rnf41 Pacs2 Pip4k2a Vmp1 Pafah1b2 Slc25a4
Npc1 Bnip3l Mapk3 Ubqln2 Gabarapl1 Ufc1 Map1lc3a
Wdr45b Arl8b Gabarapl2 Rragb Mapt Cltc Hmgb1
Myelin
Stxbp1 Cntn1 Aldoa Mag Cltc Septin8
Actb Slc25a4 Atp5a1 Dld Gdi2 Glul
Ndrg1 Dpysl2 Msn Ncam1 Prdx1 Pacsin1
Sod2 Tagln3 Ndufa10 Fyn Dag1 Epb41l3
b
AS-specific
postsynapse organization
axonogenesis
regulation of postsynaptic membrane neurotransmitter receptor levels
synapse organization
positive regulation of cell projection organization
vesicle-mediated transport in synapse
p.adjust
c
GABA receptor
Gabbr1
Gabra1
Gabra3
Gabrg2
T>C conversion (%)
4sU-
4sU+
Glutamate receptor
Gria3
Gria4
Grina
e
CS-specific
myelination
positive regulation of myelination
autophagy
regulation of intracellular transport
macroautophagy
myelin sheath
p.adjust
d
Myelination related genes
4sU+
4sU-
Fyn
Dag1
Mag
Epb41l3
Ndrg1
f
BL
CS
MBP
20 μm
g
MBP
Mean gray value
BL
CS